

Dynamic weakening by acoustic fluidization during stick-slip motion

F. Giacco^{1,2}, L. Saggese³, L. de Arcangelis^{3,4}, E. Lippiello^{2,4,*}, M. Pica Ciamarra^{5,1}

¹*CNR-SPIN, Dept. of Physics, University of Naples "Federico II", Naples, Italy*

²*Dept. of Mathematics and Physics, Second University of Naples and CNISM, Caserta, Italy*

³*Dept. of Industrial and Information Engineering,*

Second University of Naples and CNISM, Aversa (CE), Italy

⁴*Kavli Institute for Theoretical Physics, University of California, Santa Barbara, CA 93106-4030 USA*

⁵*Division of Physics and Applied Physics, School of Physical and
Mathematical Sciences, Nanyang Technological University, Singapore **

The unexpected weakness of some faults has been attributed to the emergence of acoustic waves that promote failure by reducing the confining pressure through a mechanism known as acoustic fluidization, also proposed to explain earthquake remote triggering. Here we validate this mechanism via the numerical investigation of a granular fault model system. We find that the stick-slip dynamics is affected only by perturbations applied at a characteristic frequency corresponding to oscillations normal to the fault, leading to gradual dynamical weakening as failure is approaching. Acoustic waves at the same frequency spontaneously emerge at the onset of failure in absence of perturbations, supporting the relevance of acoustic fluidization in earthquake triggering.

PACS numbers: 45.70.n, 45.70.Ht, 46.55.+d, 91.30.Px

Most fault systems exhibit a resistance to shear stress much smaller than the one predicted by experiments measuring the friction coefficient of sliding rocks [1]. A possible explanation of this unexpected observation is represented by “acoustic fluidization” (AF) that is active due to the presence of crushed and ground-up rocks produced by past wearing inside the fault, usually defined as fault gouge [2, 3]. According to the AF mechanism, seismic fracture produces elastic waves that diffuse and scatter inside the fault, generate a normal stress contrasting the confining one, and thus promote seismic failure. The same mechanism could be also activated by transient seismic waves generated by other earthquakes. AF, indeed, has been also proposed to explain why seismic activity is observed to increase, within minutes after big earthquakes, in areas at a distance of thousand kilometers from the mainshock epicenter [4–6]. Because of the large distance and the rapid response, the passage of seismic waves represents the most reasonable explanation for this remote triggering [7–9]. Indeed, these seismic waves could scatter inside a fault, effectively reducing the confining pressure and promoting failure. To investigate this scenario, experiments have considered granular based models of seismic faults [10–13], and demonstrated that acoustic perturbations can produce lasting changes in the granular rheology, together with stick-slip events [11, 12] and auto-acoustic compaction [13]. For instance, acoustic waves have been recently shown to induce up to a tenfold decrease in the frictional strength [14, 15] of granular materials. Consistently, numerical investigations have also demonstrated that vibrations can advance the time of slip instability [16, 17]. Other studies have identified a frequency regime leading to friction reduction [18, 19] caused the detachment of the particles from the vibrating confining planes and not related to the fluidization of

the granular bed.

Here we validate the AF scenario through the numerical investigation of a model system. First we show that perturbations at a characteristic resonant frequency are able to activate acoustic modes inside the fault, promoting the entire system fluidization. Then we clarify that these modes are relevant in the AF scenario as they spontaneously emerge at the onset of slip instabilities, in the absence of perturbations.

We study the AF mechanism through the numerical investigation of a granular fault model that reproduces the main statistical features of real earthquake occurrence [20, 21]. The model consists of $N = 1000$ spherical grains of mass m and diameter d , representing the fault gouge, confined between two rough rigid layers of size $L_x \times L_y = 20d \times 5d$, at constant pressure P_0 . Grains interact through a normal viscoelastic interaction and a tangential frictional one [20, 21]. Periodic boundary conditions are imposed along x and y . A stick slip dynamics is induced by driving the system via a spring mechanism. Specifically, one extreme of the spring is attached to the top plate, while the other moves along x at constant velocity v_d . Accordingly, if the plate does not move the shear stress $\sigma = \sigma_{xy}$ increases at a rate $k_d v_d / L_x L_y$, where k_d is the spring elastic constant. We measure the mass in units of m , the lengths in units of d and time in units of $\sqrt{m/k_d}$. The confining pressure is $P_0 = k_d/d$, $v_d = 0.01 d / \sqrt{m/k_d}$ and the temporal integration step of the equations of motion is $5 \cdot 10^{-3} \sqrt{m/k_d}$. For these values of the parameters, the fault width slightly fluctuates around $W \simeq 10d$ and the system exhibits a stick-slip motion [20–22], as shown in Fig. 1. We identify slips imposing a threshold 10^{-4} on the top plate velocity. We have previously shown that the slip size distribution of this model has a power law regime in agreement with the

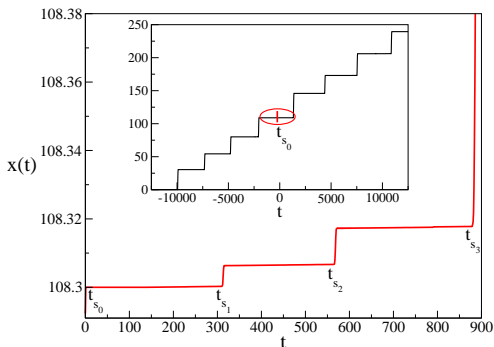


FIG. 1: (color online) Time evolution of the top plate position. The inset shows the evolution in a large time interval, while the main panel focuses on a shorter time interval following time $t_{s_0} = 0$. In this shorter interval we observe three small slips, at time t_{s_0} , $t_{s_1} = 321$ and $t_{s_2} = 576$, and a large one at time $t_{s_3} = 890$.

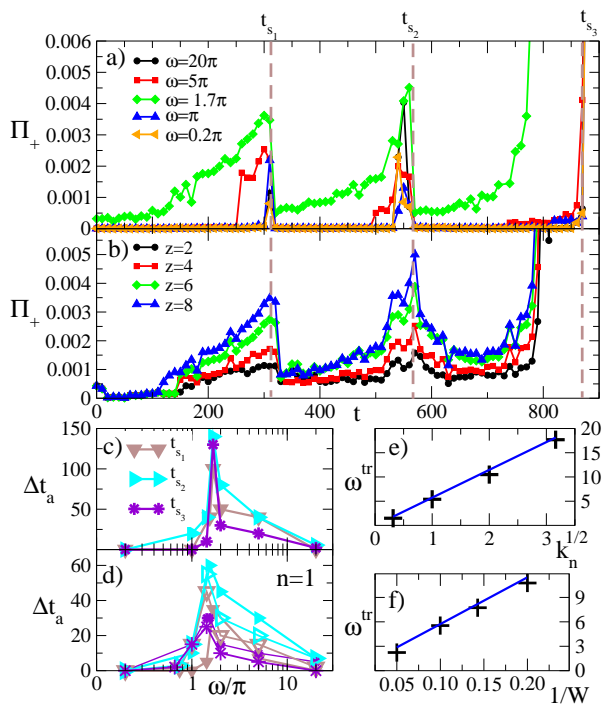


FIG. 2: (color online) (a) Time dependence of the system's response $\Pi_+(t, W - 1)$ to perturbations increasing the confining pressure, at different frequencies. (b) The response $\Pi_+(t, z)$ for grains belonging to different vertical positions z . (c) Frequency dependence of the advance time Δt_a of the slips occurring at times t_{s_1} , t_{s_2} and t_{s_3} , induced by perturbation $P_+(t)$. (d) As in panel c, for single pulse perturbations increasing the pressure (full symbols) or decreasing the shear stress (open symbols). Panels (e-f) show that the characteristic triggering frequency scales as $\omega^{\text{tr}} \propto k_n^{1/2}/W$, with k_n grain stiffness and W fault width.

Gutenberg-Richter law observed for earthquakes [20, 21], and a bump at large slips related to the system size.

In the following we focus on the temporal window

$[t_{s_0} : t_{s_3}]$ illustrated in Fig. 1, but analogous results are observed in other temporal intervals. In this time window we observe three small slips, at times $t_{s_0} = 0$, t_{s_1} and t_{s_2} , where the displacement of the top plate $\delta x(t_{s_j}) < 0.1d$ followed by a large slip, at time t_{s_3} with $\delta x(t_{s_3}) \simeq L_x$. Both small and large slips involve the rearrangement of all grains inside the fault. In particular, the velocity profile during all slips is compatible with a laminar flow indicating that slip instabilities correspond to a transition from a jammed solid-like to an unjammed fluid-like configuration. Our goal is to understand whether an acoustic perturbation can cause this fluidization, and whether in absence of perturbations spontaneous acoustic emissions occur at slip instabilities. To mimic an acoustic perturbation resulting from an incoming seismic wave, at each time t we consider a replica of the unperturbed system. Each replica is then perturbed by means of a series of n sinusoidal stress pulses of total duration τ , in absence of the external drive ($v_d = 0$). Specifically, either we force the shear stress to vary by $\sigma_{\pm}(t_p, t) = \pm \frac{\alpha \sigma(t)}{2} [1 - \sin(\frac{\pi}{2} + \omega(t_p - t))]$, or the confining pressure by $P_{\pm}(t_p, t) = \pm \frac{\alpha P_0}{2} [1 - \sin(\frac{\pi}{2} + \omega(t_p - t))]$, where t indicates that we are considering the replica taken at time t , whereas t_p refers to the time evolution of the perturbed system. We also found that purely sinusoidal perturbations lead to analogous results.

We fix the duration of each perturbation to $\tau = 10$ and consider frequencies ω leading to $n = \frac{\tau \omega}{2\pi} \in [1, 10^3]$ pulses, restricting to the linear response regime $\alpha \ll 1$. In this regime the perturbing pressure is much smaller than the confining one, and it is not able to induce the detachment of the grains from the confining plates. The situation is different from the procedure applying a mechanical vibration to the the bottom substrate as in the study of ref. [18, 19]. In this case, indeed, for a given amplitude of the applied vibration there is a range of frequency leading to the detachment from the bottom substrate. We also note that the perturbations σ_+ and P_- correspond to an increase of the shear stress and to a reduction of the confining pressure, respectively, and are thus expected to facilitate failure. Conversely the perturbations σ_- and P_+ should inhibit failure.

The perturbation leads to a global rearrangement of grains inside the system. We thus quantify the effect of the perturbation by means of the displacement $\Delta x(t, z) = x_{\alpha}(t + \tau, z) - x_0(t + \tau, z)$, where $x_{\alpha}(t + \tau, z)$ is the average position of all grains with vertical position $\in [zd, zd + d)$ after the perturbation has been applied, and $x_0(t + \tau, z) \simeq x_0(t, z)$ is their average unperturbed position. We use these displacements to estimate the frictional weakening in response to the the perturbations P_{\pm} and σ_{\pm} via the parameters $\Pi_{\pm}(t, z) = \Delta x(t, z)/\alpha P_0$ and $\Sigma_{\pm}(t, z) = \Delta x(t)/\alpha \sigma(t, z)$. In the following, we mainly focus on the top plate response $\Pi_{\pm}(t, W - 1)$ or $\Sigma_{\pm}(t, W - 1)$ and report results obtained in the linear

response regime ($\alpha < 0.05$), where P_{\pm} and σ_{\pm} are α independent.

We first consider the response to an increase of the confining pressure, expecting to observe $\Pi_+ \simeq 0$ since a pressure increase is supposed to keep a system in a jammed state. Indeed, Fig. 2a shows that for most frequencies $\Pi_+ \simeq 0$, as long as t is not very close to a slip occurrence time. However, for $\omega = 1.7\pi$ the response is significantly different than zero at all times. To investigate the frequency dependence of the response, we observe that an external perturbation applied at a time $t < t_s$ induces a displacement $\Delta x(t, W-1)$ which is smaller but comparable to the one observed in the unperturbed system when the failure occurs at time t_s , $\delta x(t_s)$. The induced displacement $\Delta x(t, W-1)$ becomes larger and larger as t approaches t_s and can be used to define the ‘advance time’, Δt_a , by the condition $\Delta x(t_s - \Delta t_a, W-1) = \beta \delta x(t_s)$. The advance time depends on both α and β , increasing with α and decreasing with β . In Fig. 2b we plot the frequency dependence of Δt_a for $\alpha = 0.02$ and $\beta = 0.2$ for all the considered slips. The behavior of Δt_a indicates that compressive perturbations trigger failure when their frequency falls in a given range, the triggering being most effective at a particular frequency, $\omega^{tr} = 1.7\pi$. For larger values of β , Δt_a converges to a delta function centered in ω^{tr} . Fig. 2c shows that analogous results are obtained when a single pulse is applied, and thus clarifies that triggering is related to the frequency of the perturbation, not to its duration. Moreover the perturbation does not only cause the displacement of the top plate but involves a non-local rearrangement of all granular layers. This is clearly enlightened by Fig. 2b where we plot the response $\Pi_+(t, z)$, at frequency ω^{tr} for different values of z . We observe that the external perturbation induces the displacement of all system layers, with a slip profile consistent with a laminar flow. Similar behavior is observed for the other temporal windows considered, with the response Π_+ monotonically increasing with the slip amplitude $\delta x(t_s)$. We also note that the magnitude of the system’s response is affected by the viscoelastic nature of the interaction between the grain, and increases (decreases) if this interaction becomes less (more) dissipative.

We interpret the above results in terms of the fluidization induced by the presence of acoustic waves scattering into the system. These waves propagate with velocity $v_a = \sqrt{M/\rho}$, where M is the P -wave modulus, and thus need a time $T_a = 2W/v_a$ to reach the bottom plate and return to the top. For a single grain under a hydrostatic pressure $M \simeq k_n/6d$, and using $\rho \simeq mN/(L_x L_y W)$ the typical AF resonant frequency is $\omega^{af} = 2\pi/T_a = (\pi/W)\sqrt{k_n/(6d\rho)}$. By performing simulations with different grain stiffnesses and system widths, we have verified that the triggering frequency is in agreement with ω^{af} , as illustrated in Fig. 2d–e. This proves that the AF mechanism is at work in the response of

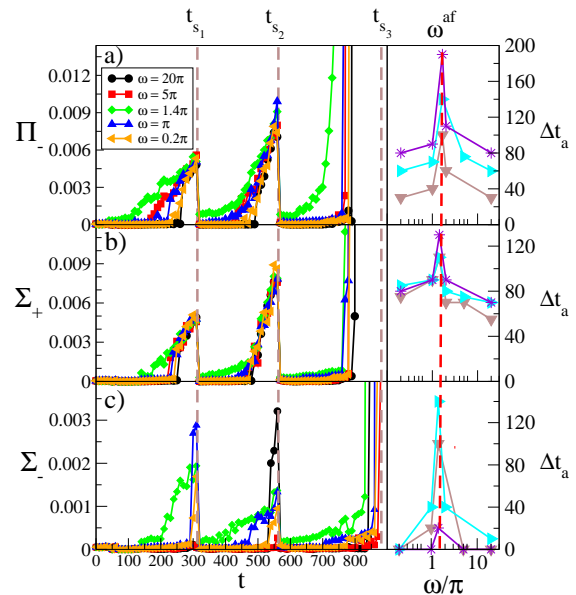


FIG. 3: (color online) The left column illustrates the response of the top plate to perturbations decreasing the confining pressure (a), increasing the shear stress (b), or decreasing the shear stress (c). The right column illustrates the frequency dependence of the advance time, which is peaked around the acoustic fluidization frequency $\omega^{af} \simeq 1.5\pi$. Symbols are as in Fig. 2b.

our system to the considered perturbation. The same conclusion is reached investigating the response to perturbations Π_- decreasing the confining pressure, as summarized in Fig. 3a. Since reducing the pressure induces failure, in this case the system is expected to be more sensitive to the perturbation, and therefore we do observe $\Pi_- > \Pi_+$ and a not-negligible response at all times. The frequency dependence of the advance time clarifies that also in this case the system is more susceptible to perturbations with a frequency close to ω^{af} , in agreement with the AF scenario.

We now analyze the response to perturbations in the shear stress, $\Sigma_{\pm}(t, W-1)$ (Fig. 3b–c). The perturbation σ_+ increases the shear stress, and it is therefore equivalent to a reduction of the time to the next slip. It is possible to show, indeed, that Σ_+ is larger for longer perturbation durations τ . For a fixed τ , as in Fig. 3b, a weak dependence on ω can be still observed with a larger response for $\omega^{tr} = 1.4\pi$. Conversely, the perturbation σ_- should inhibit the top plate displacement and therefore we would expect $\Sigma_- \simeq 0$. This is the case except at $\omega^{tr} = 1.4\pi$ where Σ_- is larger than zero in a wide temporal range. Note that the characteristic frequency observed in the response to perturbations in the shear stress is very close to that characterizing the response to perturbations applied to the pressure, and the two are found to scale in the same way with the system width and the grain stiffness. Overall, these results indi-

cate that AF can be triggered by perturbations applied along any direction, and provide a possible explanation of triggering caused by transient seismic waves regardless the fault orientation. Nevertheless, since seismic waves from remote earthquakes present small frequency signals ($\omega \lesssim 1$ Hz), assuming $v_a \sim 1$ km/sec, AF represents a realistic mechanism only for fault widths $W \gtrsim 10^3$ m, much larger than typical experimental values [3, 15]. The AF scenario can be still recovered if seismic waves are able to excite a local source of high frequency energy or if seismic wave velocity abruptly decreases entering the fault granular gouge. This velocity reduction can be attributed to spatial heterogeneity of the granular medium as measured in experiments with glass beads [23].

Having clarified the relevance of AF in the response of the system to external perturbations, we now show that acoustic emissions can spontaneously appear and weaken a fault, inducing its failure, as suggested in ref. [2]. A similar mechanism has been used to rationalize the compaction of sand grains under shear [13]. We test this hypothesis by investigating whereas, in the unperturbed system, changes in the features of particle motion suggest the emergence of acoustic waves on approaching failure. To do so, at each time t , we create a replica of the system decoupled from the external drive ($v_d = 0$) and follow its spontaneous relaxation in the subsequent time interval. We evaluate the time dependence of the power spectral density $\hat{C}(t, \omega)$ obtained from the autocorrelation function of the particle velocities \vec{v}_i ,

$$C(t, t') = \frac{\sum_{i=1}^N \vec{v}_i(t) \cdot \vec{v}_i(t')}{\sum_{i=1}^N \vec{v}_i(t) \cdot \vec{v}_i(t)}.$$

We present in Fig. 4a the map of $\log(|\hat{C}(t, \omega)|)$ for different values of ω and $t \in [0, t_{s_3} - 10]$ [24]. The dashed vertical black lines indicate the slip occurrence times t_{s_1} and t_{s_2} . Fig. 4a shows that oscillations at the characteristic frequency appear at the onset of each slip. Their amplitude then decreases roughly exponentially in time, as observed in Fig. 4b. This figure also shows that oscillations at other frequencies are essentially unaffected by the slips. This behavior is systematically observed in other slip sequences.

Figure 4 is consistent with a scenario where, as soon as acoustic oscillations spontaneously form inside the system, the confining pressure is reduced inducing slip occurrence. To investigate this hypothesis, in Fig. 5 we focus on the behavior of $|\hat{C}(t, \omega^{\text{af}})|$ in a temporal period centered at the slip occurrence time. In the figure we also plot the evolution of $C(t, t')$ as function of $t' - t$ for nine different values of t .

In temporal intervals distant from the slip occurrence times $C(t, t')$ is structureless, leading to $|\hat{C}(t, \omega^{\text{af}})| \simeq 0$. The same behavior is observed up to times $t_s - t > 2$ before the slip. Interestingly, as soon as the slip is approaching ($t_s - t < 2$), oscillations at the characteristic

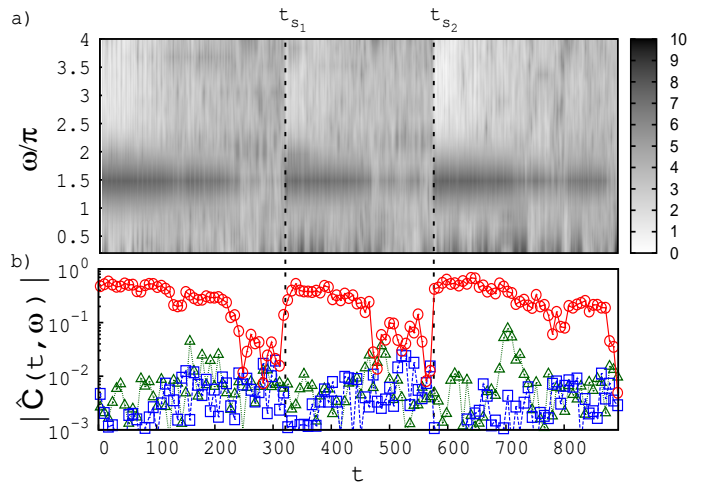


FIG. 4: (color online) (a) The map of the logarithm of the power spectral density, $|\hat{C}(t, \omega)|$ as function of t and ω . (b) Time dependence of the power spectral density at three different frequencies, $\omega \simeq \pi$ (squares), $\omega = \omega^{\text{af}} \simeq 1.5\pi$ (circles) and $\omega \simeq 2\pi$ (triangles). The dashed vertical lines indicate the slip occurrence time t_{s_1} and t_{s_2} .

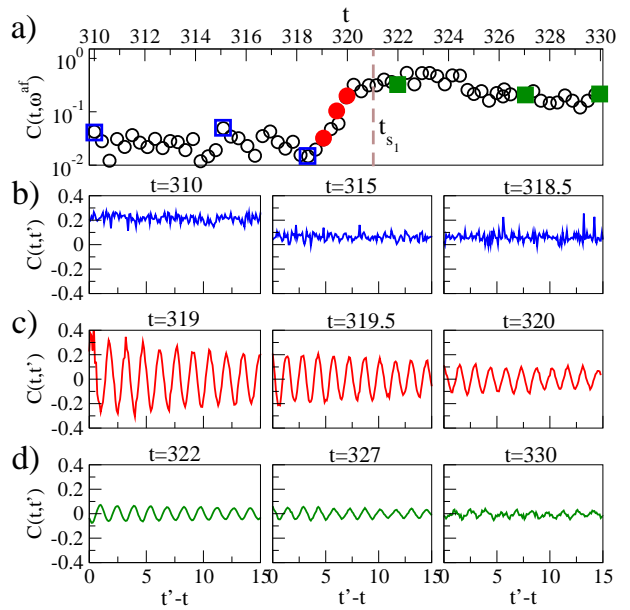


FIG. 5: (color online) (Panel a) Time dependence of the power spectral density at the characteristic frequency $|\hat{C}(t, \omega^{\text{af}})|$, in a temporal interval centered at the slip occurrence time t_{s_1} . The bottom panels illustrate the temporal evolution of $C(t, t')$ evaluated at different times t indicated in panel (a) as open blue squares for $t_{s_1} - t > 2$ (panel b), filled red circles $t_{s_1} - t < 2$ (panel c) and filled green squares $t - t_{s_1} > 2$ (panel d).

frequency ω^{af} appear in $C(t, t')$ and indeed $|\hat{C}(t, \omega^{\text{af}})|$ drastically increases. These oscillations are still present even in temporal periods after the slip, but their amplitude decreases in time. This result evidences that spontaneous oscillations appear at ω^{af} just at the onset of

the slip, favoring system failure. The same pattern is recovered for another slip at time t_{s_2} .

Summarizing, our results strongly support the validity of the AF scenario by proving that the system is susceptible to external perturbations with a characteristic frequency, and that in absence of perturbations acoustic vibrations at this characteristic frequency spontaneously emerge at the onset of failure. Accordingly, these oscillations are able to cause a slip instability regardless of their origin.

E.L. and L.d.A. acknowledge financial support from the National Science Foundation under Grant No. NSF PHY11-25915. L.S. is supported by the MASTRI EXCELLENCE NETWORK (CUP B25B09000010007) of the Campania region. M.P.C. acknowledges financial support from the CNR-NTU joint laboratory for ‘Amorphous Materials for Energy harvesting applications’.

* Corresponding author: eugenio.lippiello@unina2.it

- [1] S. H. Hickman, *Rev. Geophys.* **29**, 759 (1991).
- [2] H. Melosh, *J. Geophys. Res.* **84**, 7513 (1979).
- [3] H. Melosh, *Nature* **379**, 601 (1996).
- [4] K. R. Felzer and E. E. Brodsky, *Nature* **441**, 735 (2006).
- [5] E. E. Brodsky and J. N. van der Elst, *Annu. Rev. Earth Planet. Sci.* **42**, 317 (2014).
- [6] E. E. Brodsky, V. Karakostas, and H. Kanamori, *Geophys. Res. Lett.* **27**, 2741 (2000).
- [7] D. P. Hill, P. A. Reasenberg, A. Michael, W. J. Arabaz, G. Beroza, D. Brumbaugh, J. N. Brune, R. Castro, S. Davis, D. dePolo, et al., *Science* **260**, 1617 (1993).
- [8] J. Gomberg, P. Bodin, K. Larson, and H. Dragert, *Nature* **427**, 621 (2004).
- [9] J. Gomberg and P. A. Johnson, *Nature* **437**, 830 (2005).
- [10] P. A. Johnson and X. Jia, *Nature* **437**, 871 (2005).
- [11] P. A. Johnson, H. Savage, M. Knuth, J. Gomberg, and C. Marone, *Nature* **451**, 57 (2008).
- [12] P. A. Johnson, B. M. Carpenter, M. Knuth, B. M. Kaproth, P.-Y. L. Bas, E. G. Daub, and C. Marone, *J. Geophys. Res.* **117**, B04310 (2012).
- [13] J. N. van der Elst, E. E. Brodsky, P. L. Bas, and P. A. Johnson, *J. Geophys. Res.* **117**, B09314 (2012).
- [14] X. Jia, T. Brunet, and J. Laurent, *Phys. Rev. E* **84**, 020301 (R) (2011).
- [15] K. Xia, S. Huang, and C. Marone, *G3* **14**, 1012 (2013).
- [16] M. Griffa, B. Ferdowsi, E. G. Daub, R. A. Guyer, P. A. Johnson, C. Marone, and J. Carmeliet, *Phys. Rev. E* **87**, 012205 (2013).
- [17] B. Ferdowsi, M. Griffa, R. A. Guyer, P. A. Johnson, C. Marone, and J. Carmeliet, *Phys. Rev. E* **89**, 042204 (2014).
- [18] R. Capozza, A. Vanossi, A. Vezzani, and S. Zapperi, *Phys. Rev. Lett.* **103**, 085502 (2009).
- [19] F. Giacco, E. Lippiello, and M. P. Ciamarra, *Phys. Rev. E* **86** (2012).
- [20] M. P. Ciamarra, E. Lippiello, C. Godano, and L. de Arcangelis, *Phys. Rev. Lett.* **104**, 238001 (2010).
- [21] M. P. Ciamarra, E. Lippiello, L. de Arcangelis, and C. Godano, *Europhys. Lett.* **95**, 54002 (2011).
- [22] M. P. Ciamarra, L. de Arcangelis, E. Lippiello, and C. Godano, *Int. J. Mod. Phys. B* **23**, 5374 (2009).
- [23] Y. F. B. Andreotti and O. Pouliquen, *Granular Media: Between Fluid and Solid* (Cambridge University, Cambridge, 2013).
- [24] The function $\log(|\hat{C}(t, \omega)|)$ cannot be evaluated in the temporal period immediately preceding the largest slip ($t \leq t_{s_3}$) since during the spontaneous relaxation, even in absence of external drive, the system reaches the slip instability